CrossMark

J. Fluid Mech. (2016), *vol.* 804, *pp.* 5–23. © Cambridge University Press 2016
doi:10.1017/jfm.2016.529

Small-scale anisotropy in turbulent boundary layers

Alain Pumir[1,4,†], Haitao Xu[2,4] and Eric D. Siggia[3]

[1]Univ Lyon, Ecole Normale Supérieure de Lyon, Univ Claude Bernard, CNRS, Laboratoire de Physique, F-69342, Lyon, France

[2]Center for Combustion Energy and Department of Thermal Engineering, Tsinghua University, 100084, Beijing, China

[3]Center for Physics and Biology, Rockefeller University, New York, NY 10065, USA

[4]Max-Planck Institute for Dynamics and Self-Organisation, Göttingen, D-37077, Germany

(Received 8 May 2016; revised 8 July 2016; accepted 8 August 2016;
first published online 31 August 2016)

In a channel flow, the velocity fluctuations are inhomogeneous and anisotropic. Yet, the small-scale properties of the flow are expected to behave in an isotropic manner in the very-large-Reynolds-number limit. We consider the statistical properties of small-scale velocity fluctuations in a turbulent channel flow at moderately high Reynolds number ($Re_\tau \approx 1000$), using the Johns Hopkins University Turbulence Database. Away from the wall, in the logarithmic layer, the skewness of the normal derivative of the streamwise velocity fluctuation is approximately constant, of order 1, while the Reynolds number based on the Taylor scale is $R_\lambda \approx 150$. This defines a small-scale anisotropy that is stronger than in turbulent homogeneous shear flows at comparable values of R_λ. In contrast, the vorticity–strain correlations that characterize homogeneous isotropic turbulence are nearly unchanged in channel flow even though they do vary with distance from the wall with an exponent that can be inferred from the local dissipation. Our results demonstrate that the statistical properties of the fluctuating velocity gradient in turbulent channel flow are characterized, on one hand, by observables that are insensitive to the anisotropy, and behave as in homogeneous isotropic flows, and on the other hand by quantities that are much more sensitive to the anisotropy. How this seemingly contradictory situation emerges from the simultaneous action of the flux of energy to small scales and the transport of momentum away from the wall remains to be elucidated.

Key words: turbulence theory, turbulent boundary layers, turbulent flows

1. Introduction

In turbulent flows, which involve many length scales, the restoration of rotational symmetry (i.e. isotropy) at very small scales is one of the central postulates (Kolmogorov 1941; Landau & Lifshitz 1959). This assumption leads to a universal description of the flow, and has provided the motivation for many studies of the

† Email address for correspondence: alain.pumir@ens-lyon.fr

https://doi.org/10.1017/jfm.2016.529 Published online by Cambridge University Press

fine-scale structure of turbulent motion in explicitly homogeneous isotropic turbulent flows (Frisch 1995). Most flows of natural or engineering interest, however, have a more complicated structure (Tennekes & Lumley 1983; Pope 2000), and typically involve a shear at large scale. The expectation is therefore that the influence of the velocity gradient at large scale has a vanishingly small influence when considering velocity differences at small scales and at very large Reynolds numbers, as originally predicted by Corrsin (1958) and Lumley (1967). Experiments at very high Reynolds numbers confirm that turbulence is isotropic at very small scales, judging from the high-wavenumber properties of the velocity spectra (Saddoughi & Veeravalli 1994; Sreenivasan & Antonia 1997).

The study of mixing of a passive scalar, in the presence of a mean gradient, points, however, to a very different conclusion (Sreenivasan 1991). Numerous observations, obtained from direct numerical simulations (DNS), experiments and models alike, point to an anisotropy, induced by the large-scale gradient, persistent all the way down to the smallest scales. The scalar gradient is expelled from large regions of the flows, and concentrates in narrow cliffs, perpendicular to the direction of the mean gradients, $\boldsymbol{G}$, where the scalar varies by a large amount over a very short distance. This expulsion of the gradients from large domains of the flows is responsible for the very characteristic 'ramp-and-cliff' structure observed by recording the temperature at a fixed position in, e.g., a slightly heated wall-bounded shear flow (Sreenivasan 1991). The scalar variations are small over the 'ramps', with large jumps concentrated over small regions (in the 'cliffs'), thus leading to a highly skewed scalar gradient. Experiments (Tong & Warhaft 1994; Warhaft 2000) and DNS (Holzer & Siggia 1994; Pumir 1994) show that the skewness of the component of the scalar gradient parallel to $\boldsymbol{G}$, $\partial_\parallel \theta = \boldsymbol{G}\cdot\boldsymbol{\nabla}\theta/|\boldsymbol{G}|$, is of the order of 2, independent of the Reynolds number. This strongly contrasts with the postulate of restoration of isotropy at small scales, and, in particular, with similarity arguments (Lumley 1967), which lead to the prediction that the skewness decreases with the Reynolds number as $\propto R_\lambda^{-1}$. The solution of theoretical models (Pumir 1998; Shraiman & Siggia 2000) leads to a semiquantitative understanding of the persistence of the small-scale anisotropy in the passive scalar problem, and even provides insight into the structure of the three-point correlation function of the scalar (Mydlarski *et al.* 1998).

A possible analogy between the fluctuations of a passive scalar in the presence of a mean gradient and those of the velocity in the presence of a uniform mean shear ($\partial_y U = S$, where U is the mean field in the streamwise direction) suggests that anisotropy could be seen also at the level of odd moments of $\partial_y u$, the derivative of the streamwise velocity component u, in the direction y, parallel to the imposed mean shear (Pumir & Shraiman 1995). In fact, only a weaker manifestation of anisotropy was observed in turbulent homogeneous shear flow (THSF): the skewness decreases, as a function of the Reynolds number, although more slowly ($\propto R_\lambda^{-1/2}$) than predicted by similarity arguments ($\propto R_\lambda^{-1}$) (Corrsin 1958; Lumley 1967); however, the normalized fifth moment remains approximately constant (Garg & Warhaft 1998; Ferchichi & Tavoularis 2000; Shen & Warhaft 2000; Warhaft & Shen 2001). More recently, several other methods have been proposed to quantify anisotropy (Kurien & Sreenivasan 2000; Biferale & Vergassola 2001; Schumacher, Sreenivasan & Yeung 2003; Staicu, Vorselaars & van de Water 2003; Biferale & Procaccia 2005; Casciola *et al.* 2007), with somewhat ambiguous conclusions. We focus in the present work on the moments of $\partial_y u$.

Although THSF provides a good test problem to study the interaction between small-scale turbulent fluctuations and a mean shear flow (Pumir 1996; Schumacher &

https://doi.org/10.1017/jfm.2016.529 Published online by Cambridge University Press

Eckhardt 2000; Gualtieri *et al.* 2002; Casciola *et al.* 2003), its large-scale structure may appear as artificial. Recent work nonetheless confirms earlier observations (Pumir 1996) that the flow structure actually shares important properties with channel flows (Cardesa *et al.* 2015; Dong *et al.* 2015; Dong 2016; Sekimoto, Dong & Jimenez 2016). In this context, it is particularly interesting to consider the anisotropy issue in more realistic cases. Here, we consider the problem of restoration of isotropy at small scales in the case of a turbulent channel flow (TCF). Decades of investigation have revealed that the turbulence properties in TCF are very anisotropic in the close vicinity of the wall. Further away from the wall, over a range of scales, the mean velocity gradient $\mathrm{d}U(y)/\mathrm{d}y$, where y is the coordinate normal to the wall and U is the streamwise component of the mean velocity, varies as u_τ/y, where u_τ is the scale of the turbulent fluctuations at the wall (Landau & Lifshitz 1959; Tennekes & Lumley 1983; Pope 2000). Recent experiments have provided a wealth of information on the structure of the flow (Smits 2010; Marusic *et al.* 2013). In addition, the possibility to simulate TCF at increasingly higher resolution (Moin & Kim 1982; Kim, Moin & Moser 1987; Moser, Kim & Mansour 1999; Vreman & Kuerten 2014) provides information on the structure of the full velocity gradient tensor and on the pressure gradients, which remain extremely difficult to measure experimentally. Abe, Antonia & Kawamura (2009) and Antonia, Abe & Kawamura (2009) suggest some interesting similarities between the velocity and temperature fluctuation spectra, although the analogies do not seem to extend to the vorticity and the scalar gradient.

The present work is based on the DNS results made available on the Johns Hopkins University Turbulence Database (Li *et al.* 2008; Lee, Malaya & Moser 2013; Graham *et al.* 2014). The main question investigated here is how the strong anisotropy induced at the wall decays inside the fluid. We focus here mostly on the region sufficiently far away from the wall, where the mean velocity profile depends logarithmically on the distance from the wall, the so-called log-layer (Tennekes & Lumley 1983; Pope 2000). In particular, we investigate in this region the skewness of $\partial_y u$ in the flow, and demonstrate that the skewness is of order 1 over a wide range of values of y, consistent with previous observations (Vreman & Kuerten 2014). This skewness reveals an anisotropy of the flow, which is slightly stronger than, but otherwise qualitatively similar to, the one observed in THSF. We show explicitly, however, that this anisotropy has a very small influence on several key quantities that characterize the small-scale dynamics of turbulence. Interestingly, thanks to the relatively large range of values of y, our results suggest simple power laws for several moments of the velocity gradient tensor as a function of the distance from the wall. This work therefore shows striking differences in the influence of the large-scale shear on the small-scale statistical properties, depending on the precise moment investigated. This may explain in part the contradictory conclusions reached when trying to quantify the return to isotropy in turbulent shear flows at large Reynolds numbers.

In § 2, we briefly describe the flow, and the way in which we determined the statistical properties presented here. Elementary characterizations of the flow are presented in § 3. Section 4 is devoted to a characterization of the anisotropy of the flow, essentially in the log-layer. We characterize the alignment of vorticity or the rate of strain tensor with the main directions of the flow, as well as the fluctuations of $\partial_y u$. In particular, the asymmetry of the distribution of $\partial_y u$ is discussed in relation to THSF. In contrast, the results of § 5 indicate that the anisotropy discussed in § 4 has very little effect on quantities such as vortex stretching. Similarly, as demonstrated in § 6, the geometrical properties of the rate of strain are not sensitive to the flow anisotropy. Section 7 is devoted to a general discussion of the results.

https://doi.org/10.1017/jfm.2016.529 Published online by Cambridge University Press

2. Data resources

Our analysis was based to a large extent on the data obtained from the public Johns Hopkins Turbulence Database. Briefly, the channel flow simulation (Graham *et al.* 2014) was carried out by directly solving the Navier–Stokes equations, using techniques described in Kim *et al.* (1987) and performed with $2048 \times 512 \times 1536$ wavenumbers. The total height of the channel is equal to $2h$, where $h = 1$ in the code units, and its extensions in the streamwise and spanwise directions are $8\pi h$ and $3\pi h$ respectively. The Reynolds number based on the friction velocity, $Re_\tau = u_\tau h/\nu$, is equal to $Re_\tau = 9.997 \times 10^2$, where ν is the viscosity and $u_\tau \equiv \sqrt{2\tau_w/\rho}$ is the friction velocity based on the local shear stress at the wall, τ_w (ρ is the density of the fluid). Equivalently, the distance of the wall from the centre of the channel, h, expressed in the wall length unit, $\delta_\nu \equiv \nu/u_\tau$, is equal to ≈ 1000. As done elsewhere, we denote the coordinates in the streamwise and spanwise directions by x and z. In the direction normal to the wall, we make the coordinate y dimensionless by using δ_ν: $y^+ = y/\delta_\nu$. The solution of the fluid equations is stored in the Johns Hopkins Turbulence Database over a time interval $0 \leqslant t \leqslant 26$ in code units (corresponding to 4000 flow fields stored).

The results shown here have been obtained by averaging over 10 time slices, at $t = 2.5 + 2 \times n$, $n = 0, \ldots, 9$. The reason for not considering earlier times comes from the observation that quantities that should vanish by symmetry in the centre of the channel, such as the skewness of $\partial_y u$, turn out to be excessively large at $t = 0.5$. We explicitly checked that, from $t = 2.5$ on, the statistical properties that we discuss in this paper do not significantly change with time. This was achieved by comparing the various moments, averaged over three consecutive time frames out of the 10 time frames used.

Twenty planes were selected in the lower part of the channel ($-h \leqslant y \leqslant 0$), including the planes $y^+ = 2^n$ ($0 \leqslant n \leqslant 9$), plus a few planes in selected regions, and the centre of the channel. At each plane of constant y^+ that spanned the whole width of the flow, we extracted the three components of velocity and the nine components of the velocity derivatives. Over the size of the simulation domain, $0 \leqslant x \leqslant 8\pi$ and $0 \leqslant z \leqslant 3\pi$ (up to periodicity), the data were obtained over a uniform grid, with $\Delta x = \Delta z = \pi/200$. This led to a total of $3 \times 8 \times (200)^2 = 9.6 \times 10^5$ points saved at each time step, at each plane. As a result, each average over a value of y has been obtained with $\sim 10^7$ data points.

We occasionally compared the results obtained in TCF with those corresponding to homogeneous isotropic turbulent (HIT) flows. To this end, we used the HIT simulations from the Johns Hopkins Turbulence Database at a Reynolds number $R_\lambda = 430$.

As explained in the introduction, our work explores analogies between TCF and THSF. The data shown here on the latter flow were obtained by running the code described in Pumir & Shraiman (1995) and Pumir (1996), at a resolution of $320 \times 160 \times 160$, on the workstations in the Physics Laboratory at the ENS Lyon. The Reynolds number of the flow, $Re = (2\pi)^2 S/\nu \approx 10^4$, corresponds to a Taylor Reynolds number, based on the streamwise component of velocity, $R_\lambda \approx 145$. Statistics were accumulated over a total time T_r, with $S \times T_r \gtrsim 100$.

3. Elementary characterization of the flow

The quality of the data can be judged by computing elementary statistical properties of the flow, such as the mean value, $U(y)$, and by determining the terms involved in

https://doi.org/10.1017/jfm.2016.529 Published online by Cambridge University Press

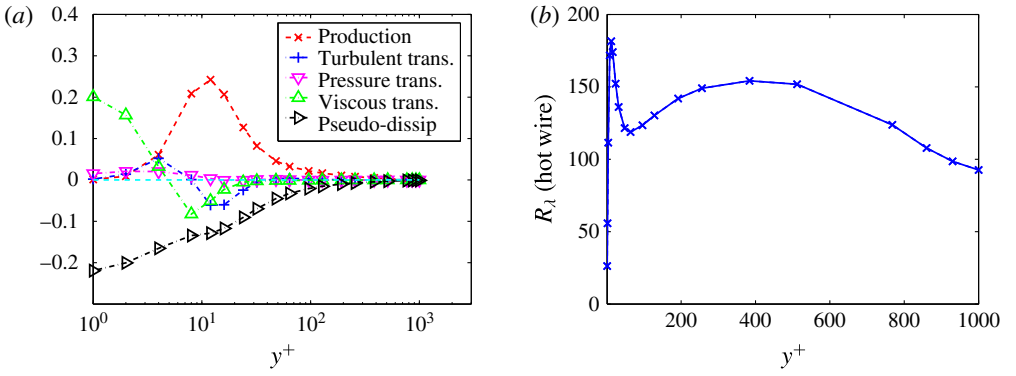


FIGURE 1. (Colour online) Characterization of the flow. (*a*) The various terms in the equation of production of kinetic energy in (3.1) as a function of the distance from the wall, y^+, all made dimensionless by dividing by u_τ^3/δ_ν. The sum of all of the terms is less than 5×10^{-3} in the dimensionless units used in the code. (*b*) The Reynolds number, as deduced from measurement of the streamwise velocity fluctuations, see the text, shows a plateau in the range $200 \lesssim y^+ \lesssim 650$.

the energy budget, which reads, in the steady state (Pope 2000),

$$-\langle uv\rangle \frac{\mathrm{d}U(y)}{\mathrm{d}y} - \frac{\mathrm{d}}{\mathrm{d}y}\left\langle \frac{1}{2} v \boldsymbol{u}^2 \right\rangle - \frac{\mathrm{d}}{\mathrm{d}y}\langle vp\rangle - \tilde{\varepsilon} + \nu \frac{\mathrm{d}^2 k}{\mathrm{d}y^2} = 0, \tag{3.1}$$

where $\boldsymbol{u} = (u, v, w)$ and p are the velocity and pressure fluctuations. The terms in (3.1) are respectively the production term by the mean shear, the turbulent and the pressure transport, the pseudo-dissipation $\tilde{\varepsilon} \equiv \nu\langle(\partial_i u_j)^2\rangle$ and the viscous transport (k is the kinetic energy, and depends on the coordinate normal to the wall, y^+, as does $\tilde{\varepsilon}$). Overall, the terms in (3.1), normalized by u_τ^3/δ_ν, shown in figure 1(*a*) are qualitatively consistent with data shown at lower Reynolds numbers, see, e.g., Pope (2000). We checked that the energy balance equation is satisfied to better than 5×10^{-3} in the dimensionless units used in figure 1(*a*). We also note that in the so-called log-layer, the two dominant terms in (3.1) are the production terms by the mean shear, $-\langle uv\rangle(\mathrm{d}U(y)/\mathrm{d}y)$, and the pseudo-dissipation term, $\tilde{\varepsilon}$.

The intensity of turbulence in homogeneous isotropic flow is characterized by the Reynolds number based on the Taylor microscale. This quantity can be expressed in terms of the longitudinal velocity, u, and its derivative with respect to the streamwise coordinate x, which can both be determined experimentally using hot wire anemometry: $R_\lambda = \langle u^2\rangle/(\nu\langle(\partial_x u)^2\rangle^{1/2})$. This definition has also been used in THSF (Garg & Warhaft 1998; Shen & Warhaft 2000). Figure 1(*b*) shows the corresponding value of the Reynolds number R_λ as a function of y^+. Consistent with Vreman & Kuerten (2014) we find that the Reynolds number determined in this way shows a sharp peak close to the wall, where the flow is very anisotropic, and a broad plateau for $200 \lesssim y^+ \lesssim 650$, with a value of R_λ larger than $\approx$140. The results shown in figure 1(*b*) are generally consistent with those of Vreman & Kuerten (2014), obtained at $R_\tau \approx 590$, with a slightly smaller value of R_λ ($R_\lambda \approx 100$) than the one found here. In qualitative agreement with Vreman & Kuerten (2014), we find that the value of R_λ based on the fluctuations of the streamwise velocity is higher than the one obtained by using a definition of R_λ based on $\langle \boldsymbol{u}^2\rangle$ and $\langle \boldsymbol{\omega}^2\rangle$ as if the flow were isotropic.

https://doi.org/10.1017/jfm.2016.529 Published online by Cambridge University Press

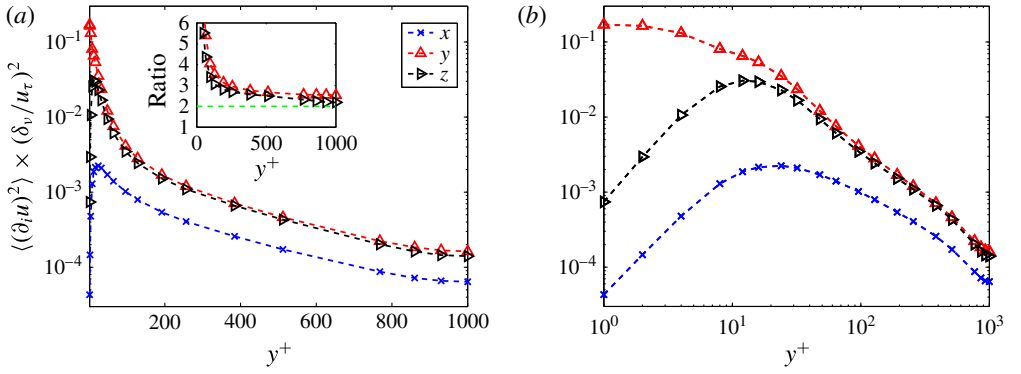


FIGURE 2. (Colour online) The second moments of the derivatives of the streamwise velocity, along the coordinates in the streamwise (crosses), normal (upper pointing triangles) and spanwise (right pointing triangles) directions, as a function of the distance from the wall, y^+; (*a*) linear scale of y^+ and (*b*) logarithmic scale of y^+. The ratios $\langle(\partial_y u)^2\rangle/\langle(\partial_x u)^2\rangle$ and $\langle(\partial_z u)^2\rangle/\langle(\partial_x u)^2\rangle$, shown in the inset of (*a*), decrease towards 2 towards the centre of the channel.

4. Small-scale anisotropy

4.1. *Alignment of the vorticity and rate of strain tensor with the flow directions*

It has been documented that the properties of the flow measured by the second moments of the velocity derivatives tend to become isotropic (Saddoughi & Veeravalli 1994). Isotropy implies that the second moments of the derivatives of $\partial_{x_i} u$ satisfy $\langle(\partial_y u)^2\rangle \approx \langle(\partial_z u)^2\rangle \approx 2\langle(\partial_x u)^2\rangle$. While this property does not have any reason to hold very close to the wall, it tends to become better satisfied when the value of y^+ increases, away from the wall; see figure 2. In particular, the ratios $\langle(\partial_y u)^2\rangle/\langle(\partial_x u)^2\rangle$ and $\langle(\partial_z u)^2\rangle/\langle(\partial_x u)^2\rangle$ decay from a value $\approx$2.9 when $y^+ = 192$ to a value $\approx$2.35 at the centre of the channel; see the inset of figure 2(*a*).

Even at the level of second moments, however, the TCF still shows signs of anisotropy away from the wall, in the log-layer ($y^+ \gtrsim 200$). Such a manifestation can be clearly seen by measuring the moments of vorticity $\langle\omega_i\omega_j\rangle$. In THSF, it is found that the component of vorticity in the direction $\boldsymbol{e}_{\pi/4} = (\boldsymbol{e}_x + \boldsymbol{e}_y)/\sqrt{2}$ (at an angle $\pi/4$ in the (x, y) plane) is significantly larger than the component of vorticity in the direction $\boldsymbol{e}_{3\pi/4} = (\boldsymbol{e}_y - \boldsymbol{e}_x)/\sqrt{2}$ (at an angle $3\pi/4$ in the (x, y) plane); the ratio between the two decreases as the Reynolds number increases (Pumir 1996). The corresponding quantities $\langle(\boldsymbol{\omega}\cdot\boldsymbol{e}_{\pi/4})^2\rangle$ and $\langle(\boldsymbol{\omega}\cdot\boldsymbol{e}_{3\pi/4})^2\rangle$ in the log-layer of the TCF are shown in figure 3. For $y^+ \gtrsim 200$, the ratio between the two quantities is comparable to what was found in turbulent shear flows at comparable Reynolds numbers; it decreases from $\approx$1.87 at $y^+ = 192$ down to $\approx$1.66 at $y^+ = 512$, to a value close to 1 at the centre of the channel. It should be noted that close to the wall ω is strongly aligned with the spanwise (z) direction, even more pronounced than the alignments shown in figure 3(*a*).

Another characterization of the small-scale properties of the flow involves the rate of strain tensor, $\boldsymbol{S}$, defined by $S_{ij} = (\partial_i u_j + \partial_j u_i)/2$. As $\boldsymbol{S}$ is a symmetric matrix, it has three real eigenvalues, denoted by λ_i, which are sorted here in decreasing order: $\lambda_1 \geqslant \lambda_2 \geqslant \lambda_3$. The incompressibility constraint imposes that $\lambda_1 + \lambda_2 + \lambda_3 = 0$. The associated eigenvectors of $\boldsymbol{S}$ are denoted as $\boldsymbol{e}_i$, with $i = 1$, 2 and 3, and $|\boldsymbol{e}_i| = 1$.

https://doi.org/10.1017/jfm.2016.529 Published online by Cambridge University Press

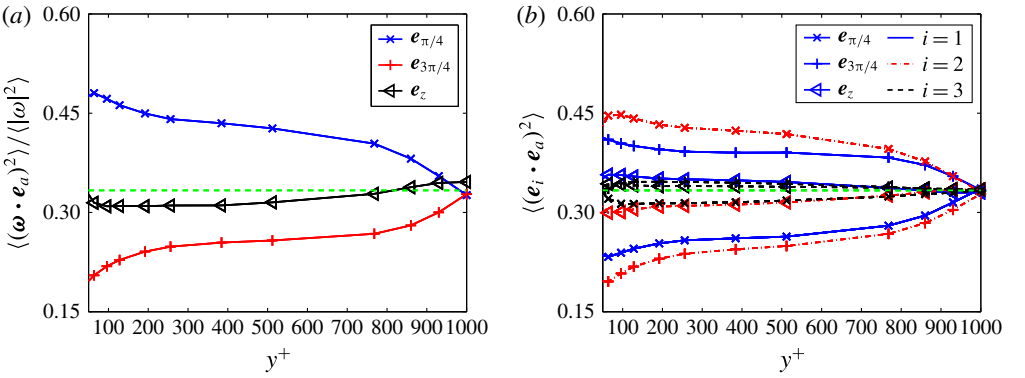


FIGURE 3. (Colour online) Alignment of the vorticity (*a*) and of the eigenvectors of strain $\boldsymbol{S}$ (*b*) with the direction of the flow. The strongest alignments of vorticity and strain are with the directions $\boldsymbol{e}_{\pi/4} = (\boldsymbol{e}_x + \boldsymbol{e}_y)/\sqrt{2}$ and $\boldsymbol{e}_{3\pi/4} = (\boldsymbol{e}_y - \boldsymbol{e}_x)/\sqrt{2}$. (*a*) The component of vorticity in the direction $\boldsymbol{e}_{\pi/4}$ is significantly larger than in the direction $\boldsymbol{e}_{3\pi/4}$, but isotropy is restored at the centre. (*b*) The eigenvector corresponding to the intermediate eigenvalue of $\boldsymbol{S}$, $\boldsymbol{e}_2$, is preferentially aligned with $\boldsymbol{e}_{\pi/4}$, whereas the eigenvector $\boldsymbol{e}_1$ is preferentially aligned with $\boldsymbol{e}_{3\pi/4}$. In comparison, $\boldsymbol{e}_3$ does not show any particular alignment with the flow directions.

Isotropy implies that the eigenvectors $\boldsymbol{e}_i$ should not show any particular alignment with the flow direction. As was the case for the vorticity, we also find a preferential alignment of the eigenvalues of strain with the directions of the flow. In particular, we find that in the log-layer ($y^+ \gtrsim 200$), the eigenvector corresponding to the largest eigenvalue of $\boldsymbol{S}$ preferentially aligns with $\boldsymbol{e}_{3\pi/4}$, whereas the intermediate eigenvector $\boldsymbol{e}_2$ preferentially aligns with $\boldsymbol{e}_{\pi/4}$. In comparison, the third eigenvector $\boldsymbol{e}_3$ does not show a strong alignment with any of the flow directions. We will return to these properties in § 6.

Thus, although the study of the partial derivatives $\partial_i u$ suggests that the flow is close to isotropy, the conclusion of this subsection is that at the Reynolds number of the flow, the vorticity and strain are aligned with some particular directions of the flow, in particular with $\boldsymbol{e}_{\pi/4}$ and $\boldsymbol{e}_{3\pi/4}$.

4.2. *Third moment of* $\partial_y u$

We consider here the third moment of the derivative of u with respect to the normal direction, which in THSF turned out to be very sensitive to the anisotropy resulting from the mean flow. In TCF, we also find a strong value of the third moment, as is illustrated in figure 4(*a*), which shows the normalized third moment of $\partial_y u$, the skewness, defined as $S_{\partial_y u} = \langle(\partial_y u)^3\rangle/\langle(\partial_y u)^2\rangle^{3/2}$, as a function of the distance from the wall. The main observation is that the skewness is approximately constant, and equal to $\approx$1.07 (see the dot-dashed line in figure 4*a*), from $200 \lesssim y^+ \lesssim 750$. At the centre of the channel, $y^+ \approx 1000$, the skewness goes to 0, which is a consequence of the symmetry at this particular point. In contrast, a much higher value of the skewness is observed at $y^+ \approx 30$, in the so-called buffer layer, where the flow is notoriously very far from isotropy. For comparison, the normalized fourth moment of $\partial_y u$, the flatness, shown in figure 4(*b*), increases slightly from the beginning of the log-layer up to the centre of the channel.

https://doi.org/10.1017/jfm.2016.529 Published online by Cambridge University Press

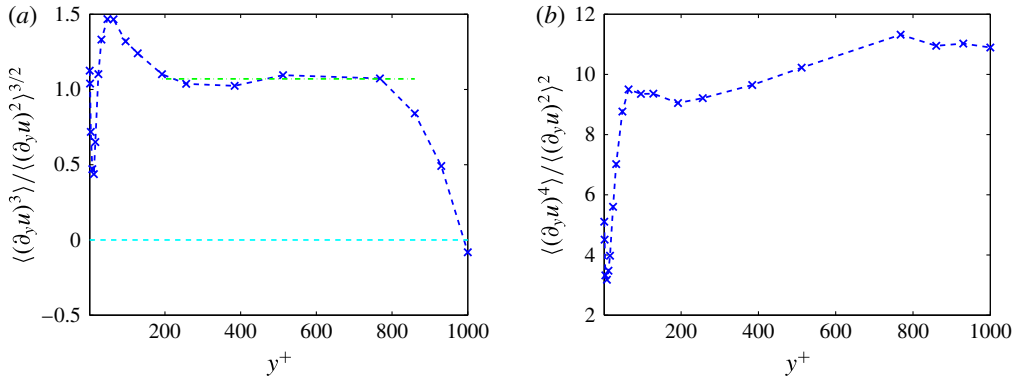


FIGURE 4. (Colour online) The third (*a*) and fourth (*b*) moments of $\partial_y u$, normalized by its root mean square. The normalized third moment (the skewness) is approximately constant over most of the channel, starting at $y^+ \approx 200$, which is at the beginning of the log-layer, up to approximately 3/4 of the overall channel width. The value indicated by the horizontal dashed–dotted line is 1.07. The skewness returns to 0 at the centre of the channel ($y^+ \approx 1000$). The normalized fourth moment (the flatness) slightly increases over the same range of values of y^+, and goes to a constant ≈11 at the centre of the channel.

We note that the properties of the moments of $\partial_y u$ are very similar to those of the moments of the spanwise component of the vorticity, $\omega_z = (\partial_x v - \partial_y u)$. In particular, the skewness $S_{\omega_z} \equiv \langle\omega_z^3\rangle/\langle\omega_z^2\rangle^{3/2}$ is approximately constant in the range $200 \lesssim y^+ \lesssim 750$, corresponding to a value $S_{\omega_z} \approx -0.85$.

It is interesting to contrast the values of the skewness of $\partial_y u$ and ω_z obtained in previous DNS calculations (Pumir & Shraiman 1995; Pumir 1996) or experimental studies of THSF (Garg & Warhaft 1998; Shen & Warhaft 2000). At small Reynolds numbers ($R_\lambda \lesssim 100$), achieved in previously published DNS at limited spatial resolution (Pumir & Shraiman 1995; Pumir 1996), the values of the skewness of $\partial_y u$ and ω_z are observed to be approximately constant, of the order of 0.84 and −0.55 respectively. At higher Reynolds numbers accessed experimentally, the skewness of $\partial_y u$ is found to decrease from values of ≈0.8 at $R_\lambda \approx 100$, with a power law dependence on the Reynolds number $S_{\partial_y u} \propto R_\lambda^{-1/2}$. The skewness of ≈0.65 that we find in the DNS of the THSF at $R_\lambda = 145$ is consistent with this law. The values obtained in the case of turbulent channel flow are certainly higher than those observed in THSF (see also § 7).

4.3. *Probability distribution functions of $\partial_y u$ and gradient expulsion*

The skewness and the flatness of $\partial_y u$ shown in figure 4 indicate that the probability distribution functions (PDFs) of $\partial_y u$ have extended tails, and exhibit a strong asymmetry. This can be directly seen in figure 5(*a*), which shows the PDF of $\partial_y u$, normalized by $\langle(\partial_y u)^2\rangle^{1/2}$, at several values of the distance from the wall, in the range $128 \leqslant y^+ \leqslant 768$. The positive tails of the PDFs vary only slightly as a function of the distance from the wall in the range shown, whereas the negative tails tend to extend further when y^+ increases.

All of the PDFs shown in figure 5(*a*) peak at values of $\partial_y u$ smaller than 0, a situation reminiscent of what was observed in THSF (Pumir & Shraiman 1995; Pumir 1996), and for the scalar. In quantitative terms, it was found that the PDF of $\partial_y u$ peaked at a value $\partial_y u \approx -0.6S$, where S is the mean shear. Figure 5(*b*) shows the

https://doi.org/10.1017/jfm.2016.529 Published online by Cambridge University Press

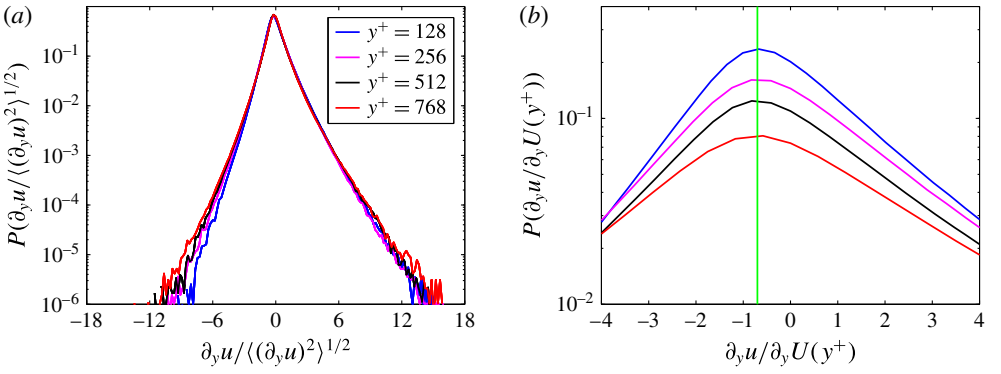


FIGURE 5. (Colour online) The PDFs of the derivative $\partial_y u$ at several locations away from the wall and from the centre: $128 \leqslant y^+ \leqslant 768 \approx 3h/4$. The PDFs normalized by the root mean square of the fluctuating quantities (*a*) superpose very well, except at $y^+ = 128$, where the probability of observing large negative fluctuations is smaller than at larger values of y^+. The PDFs normalized by the mean gradient $U'(y)$ (*b*) show that the PDFs of $\partial_y u$ peak at a value $\approx -0.7U'$. This can be interpreted as a partial expulsion of the gradient, more significant than what has been observed in THSF.

PDF of $\partial_y u$, divided by the mean velocity gradient $U'(y^+)$, blown up near $\partial_y u = 0$. The maximum of the curves is observed to peak at a value of ≈ -0.7, slightly higher than observed in THSF. Even though $U'(y^+) \sim 1/y^+$, all curves peak at the same point in rescaled units.

The peak of the PDF of $\partial_y u$ at a value close to $\approx -0.7U'(y^+)$ implies that the derivative with respect to the distance from the wall of the streamwise velocity component, $\partial_y(U + u)$, has its largest probability at a value that is significantly reduced compared with the mean gradient $U'(y^+)$.

In the problem of a passive scalar with a mean gradient, the PDF of the scalar gradient strongly peaks at 0 (Holzer & Siggia 1994; Pumir 1994; Tong & Warhaft 1994). This corresponds to the simple physical picture of a scalar field approximately constant over large domains of the flow, from which the gradient is 'expelled'. These regions are separated by narrow cliffs, where strong scalar variations concentrate (Holzer & Siggia 1994; Pumir 1994). A similar, although weaker, expulsion mechanism was observed in the case of THSF (Pumir & Shraiman 1995; Pumir 1996). In TCF, a similar phenomenon can be observed, as illustrated in figure 6, which shows the instantaneous velocity profile at several locations along the streamwise direction (x), in a given (x, y) plane, corresponding to a fixed spanwise location. The full curves show the actual velocity profile $U(y) + u(x, y)$ as a function of y (vertical), the curves corresponding to different values of x being shifted by a quantity proportional to x. For comparison, the dashed curves show the mean velocity profile, which is independent of x in the fully developed channel flow considered here, shifted by the same quantity as the instantaneous velocity. Figure 6 thus suggests the existence of regions with a streamwise velocity close to constant, separated by steep cliffs. The sharpest one in figure 6 is found at a value $y^+ \approx 200$, while smaller ones are visible at different distances from the wall. These structures are comparable to those presented in the case of homogeneous shear flows (Pumir & Shraiman 1995; Pumir 1996). We stress that figure 6 provides a physical illustration of the quantitative observations concerning the distribution of $\partial_y u$.

https://doi.org/10.1017/jfm.2016.529 Published online by Cambridge University Press

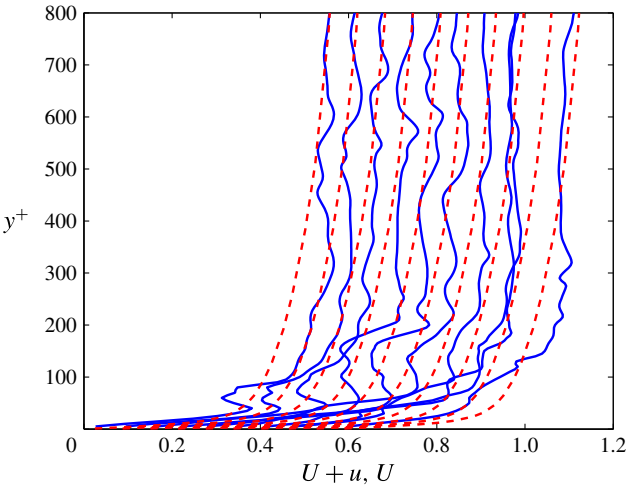


FIGURE 6. (Colour online) Snapshot of the instantaneous velocity profile, at a particular instant of time, in an (x, y) plane. The full lines show the velocity, $U+u$. For comparison, the dashed lines show the mean velocity profile as a function of y. The cliff and ramp structure is visible, as it was visible in TSHF (Pumir & Shraiman 1995; Pumir 1996). Two consecutive traces are separated by $\Delta x = 2\pi/100$.

5. Invariants of the velocity gradient tensors and implications for turbulent production

While the results presented in § 4 show a strong anisotropy of the velocity field, other characterizations of the TCF flow involving scalar combinations of velocity gradients are remarkably similar to HIT. We define the velocity gradient $A_{ij} = \partial_i u_j$ and its decomposition into strain and vorticity, $A_{ij} = S_{ij} - \epsilon_{ijk}\omega_k/2$. We begin with two examples that we understand analytically.

5.1. *Second- and third-order invariants of the velocity gradient tensor*

In homogeneous flows, the two quantities $A_2 \equiv \langle A_{ij}A_{ji}\rangle$ and $A_3 \equiv \langle A_{ij}A_{jk}A_{ki}\rangle$ are known to be identically 0 (Betchov 1956). Using the fact that $A_2 = \langle \mathrm{tr}(\boldsymbol{S}^2)\rangle - \langle \boldsymbol{\omega}^2\rangle/2$ and $A_3 = \langle \mathrm{tr}(\boldsymbol{S}^3)\rangle + 3/4\langle \boldsymbol{\omega}\cdot\boldsymbol{S}\cdot\boldsymbol{\omega}\rangle$, these relations provide kinematic constraints between strain and vorticity and between strain skewness and vortex stretching, $\langle \boldsymbol{\omega}\cdot\boldsymbol{S}\cdot\boldsymbol{\omega}\rangle$. In a highly inhomogeneous case, such as a turbulent boundary layer, it may be expected that A_2 and A_3 deviate significantly from 0. A deviation from $A_2 = 0$ would indicate an imbalance between strain and vorticity, whereas a deviation from $A_3 = 0$ would point to a difference between vortex stretching, $\langle \boldsymbol{\omega}\cdot\boldsymbol{S}\cdot\boldsymbol{\omega}\rangle$, and the strain skewness, $\langle \mathrm{tr}(\boldsymbol{S}^3)\rangle$.

We determined numerically the values of A_2 and A_3 as a function of y^+, and found that both A_2 and A_3 are remarkably small throughout the entire width of the channel. In quantitative terms, A_2 is negative for $y^+ \lesssim 16$, and positive otherwise. The most negative value of $A_2/\langle \mathrm{tr}(\boldsymbol{S}^2)\rangle$ is ≈ -0.06 (for $y^+ \approx 5$) and the most positive value is ≈ 0.025 (for $y^+ \approx 32$). Similarly, the value of A_3 is positive for $y^+ \lesssim 10$ and negative otherwise; its magnitude is smaller than $\approx 6\,\%$ of the magnitude of $\langle \mathrm{tr}(\boldsymbol{S}^3)\rangle$.

It follows from these results that the relations known to hold in homogeneous turbulence, $\langle \mathrm{tr}(\boldsymbol{S}^2)\rangle = \langle \boldsymbol{\omega}^2\rangle/2$ and $\langle \mathrm{tr}(\boldsymbol{S}^3)\rangle = -3/4\langle \boldsymbol{\omega}\cdot\boldsymbol{S}\cdot\boldsymbol{\omega}\rangle$, are very nearly satisfied

https://doi.org/10.1017/jfm.2016.529 Published online by Cambridge University Press

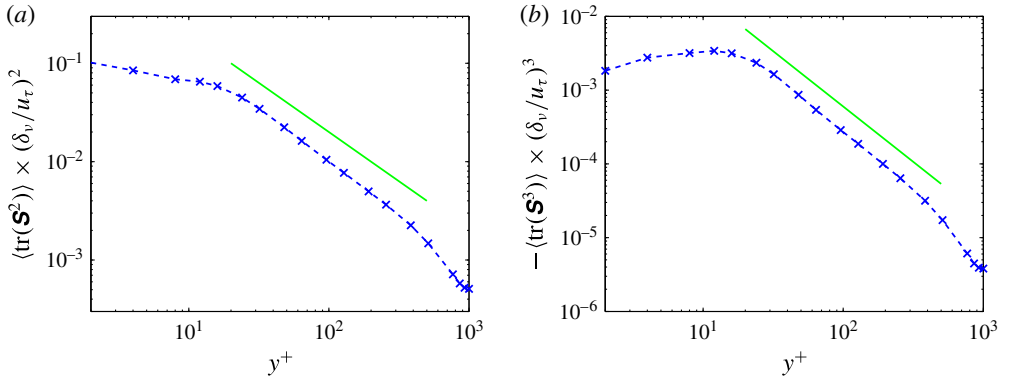


FIGURE 7. (Colour online) The averages $\langle \mathrm{tr}(\boldsymbol{S}^2)\rangle$ (*a*) and $\langle \mathrm{tr}(\boldsymbol{S}^3)\rangle$ (*b*) as a function of the distance from the wall, y^+. The two quantities decay with an approximate power law away from the wall, for $30 \lesssim y^+ \lesssim 500$. The straight lines correspond to power laws with exponents -1.14 (*a*) and -1.5 (*b*). As a result, the dimensionless ratio $\langle \mathrm{tr}(\boldsymbol{S}^3)\rangle/\langle \mathrm{tr}(\boldsymbol{S}^2)\rangle^{3/2}$ slightly increases away from the wall.

in the turbulent channel flow. The first of these relations was already noted to hold approximately in TCF by Bradshaw & Perot (1993), where they showed that $A_2 = \partial^2\langle v^2\rangle/\partial y^2$.

As the variations of mean quantities are typically much smaller than averages of the gradients of fluctuating fields, A_2 is effectively much smaller than $\langle \mathrm{tr}(\boldsymbol{S}^2)\rangle$. Similarly, elementary algebra shows that the third moment A_3 can be expressed as $A_3 = (1/2)\partial^3\langle v^3\rangle/\partial y^3 - (3/2)\partial\langle v\,\mathrm{tr}(\boldsymbol{A}^2)\rangle/\partial y$, thus explaining the numerical observation that A_3 is much smaller than $\langle \mathrm{tr}(\boldsymbol{S}^3)\rangle$.

As explained in Bradshaw & Perot (1993), the significance of the small value of A_2 is that the kinetic energy dissipation term can be expressed equivalently in terms of $\langle \boldsymbol{\omega}^2\rangle$ or in terms of the strain $\langle \mathrm{tr}(\boldsymbol{S}^2)\rangle$, up to very small corrections. Similarly, the small value of A_3 implies that the overall production of velocity gradients by turbulence can be expressed equivalently in terms of vortex stretching, $\langle \boldsymbol{\omega}\cdot\boldsymbol{S}\cdot\boldsymbol{\omega}\rangle$, or in terms of the third moment of $\boldsymbol{S}$, $\langle \mathrm{tr}(\boldsymbol{S}^3)\rangle$. This is a direct consequence of the Navier–Stokes equations, which lead to the following expression for the production of velocity gradients, $\sum_{i,j=1}^{3}(\partial_i u_j)^2 = \mathrm{tr}(\boldsymbol{A}\cdot\boldsymbol{A}^{\mathrm{T}})$:

$$\frac{\mathrm{d}}{\mathrm{d}t}\langle \boldsymbol{A}\cdot\boldsymbol{A}^{\mathrm{T}}\rangle + 2\langle \mathrm{tr}(\boldsymbol{A}^2\boldsymbol{A}^{\mathrm{T}})\rangle = \mathrm{RHS}, \tag{5.1}$$

where the RHS term contains contributions from viscosity (dissipation), pressure, transport by the fluctuations and interaction with the mean flow (Pope 2000). Away from the wall region, for $y^+ \gtrsim 100$, the nonlinear term in (5.1) dominates over all of the other contributions (Pope 2000; Vreman & Kuerten 2014). Therefore, using the relation $\langle \mathrm{tr}(\boldsymbol{A}^3)\rangle \approx 0$, one obtains for $y^+ \gtrsim 100$ the following approximate relation $\langle \mathrm{tr}(\boldsymbol{A}^2\boldsymbol{A}^{\mathrm{T}})\rangle \approx -\langle \boldsymbol{\omega}\cdot\boldsymbol{S}\cdot\boldsymbol{\omega}\rangle \approx (4/3)\langle \mathrm{tr}(\boldsymbol{S}^3)\rangle$. This in turn leads to the conclusion that away from the wall, small-scale production is expressed in terms of vortex stretching, as is the case in homogeneous isotropic flows.

Figure 7 shows the second and third moments of $\boldsymbol{S}$ as a function of the distance from the wall. We observe that, as was the case in homogeneous isotropic flows, the moment $\langle \mathrm{tr}(\boldsymbol{S}^3)\rangle$ is negative, which is related to the positive sign of vortex stretching,

https://doi.org/10.1017/jfm.2016.529 Published online by Cambridge University Press

$\langle \boldsymbol{\omega} \cdot \boldsymbol{S} \cdot \boldsymbol{\omega} \rangle > 0$. We find that both $\langle \mathrm{tr}(\boldsymbol{S}^2) \rangle$ and $-\langle \mathrm{tr}(\boldsymbol{S}^3) \rangle$ have approximate power law dependences in the log-layer, with power laws close to $y^{+\alpha_2}$ and $y^{+\alpha_3}$ for the second and third moments respectively. The exponent α_3 is very close to $-3/2$; see figure 7(*b*). The data shown in figure 7(*a*) suggest a value of α_2 close to -1: $\alpha_2 \approx -1.14$. In general, the exponents α_2 and α_3 can be approximately estimated by using the relation $\tilde{\varepsilon} \approx u_\tau^3 / y^+$, which can be deduced by balancing the dissipation $\tilde{\varepsilon}$ with the production term $U'(y) \times \langle uv \rangle$ (see Brouwers 2007). As a result, the dimensionless ratio $\langle \mathrm{tr}(\boldsymbol{S}^3) \rangle / \langle \mathrm{tr}(\boldsymbol{S}^2) \rangle^{3/2}$ is approximately constant for $y^+ \gtrsim 20$, up to the centre of the channel (with a small decrease from ≈ -0.25 in the buffer layer to ≈ -0.32 at the centre). These values are generally consistent with the value of $\langle \mathrm{tr}(\boldsymbol{S}^3) \rangle / \langle \mathrm{tr}(\boldsymbol{S}^2) \rangle^{3/2}$ in HIT, where this dimensionless ratio is equal to $(7/4)(2/15)^{1/2} S_{\partial_x u_x}$, with $S_{\partial_x u_x} = \langle (\partial_x u_x)^3 \rangle / \langle (\partial_x u_x)^2 \rangle^{3/2}$ being of the order of 0.5, which equals that in the centre of the channel to a few per cent.

The results in this subsection suggest that the anisotropy that is very visible at the level of the derivative $\partial_y u$ does not much affect the second- and third-order moments which are invariant under rotations (this is consistent with the results of Cardesa *et al.* (2013)). This may be related to the observation that the third moment $\langle (\partial_y u)^3 \rangle$ does not enter any of the expressions of the low-order moments considered here.

5.2. *Higher-order invariants*

In homogeneous and isotropic turbulence, the fourth-order velocity tensor can be fully characterized by four independent quantities that are explicitly invariant under rotation (Siggia 1981):

$$\left.\begin{aligned} I_1 &= \langle \mathrm{tr}(\boldsymbol{S}^2)^2 \rangle, \\ I_2 &= \langle (\boldsymbol{\omega}^2) \mathrm{tr}(\boldsymbol{S}^2) \rangle, \\ I_3 &= \langle \boldsymbol{\omega} \cdot \boldsymbol{S}^2 \cdot \boldsymbol{\omega} \rangle, \\ I_4 &= \langle (\boldsymbol{\omega}^2)^2 \rangle. \end{aligned}\right\} \tag{5.2}$$

These invariants are shown in figure 8 for TCF. The dependence of the fourth-order moments $I_1, \ldots, I_4$ as a function of the distance from the wall, y^+, is shown in figure 8(*a*). Away from the wall region, for $y^+ \gtrsim 20$, the dependence of the fourth-order invariants on y^+ is very close to a power law with an exponent -2.1, approximately valid for $20 \lesssim y^+ \lesssim 700$. This is again close to the value of -2 expected for $\tilde{\varepsilon}^2$. Figure 8(*b*) shows three ratios formed by normalizing with I_1. The ratios I_2/I_1 and I_3/I_1 are both essentially constant over a wide range of values of y^+, and equal respectively to $\approx$1.68 and $\approx$0.235. In comparison, the ratio I_4/I_1 increases slightly throughout the entire width of the channel. The value indicated in figure 8(*b*) is equal to 7. The values of the ratios I_2/I_1 and I_3/I_1 are fully consistent with the values reported for HIT (Ishihara *et al.* 2007): $I_2/I_1 \approx 1.75$, $I_3/I_1 \approx 0.230$. The value found in HIT, $I_4/I_1 \approx 8$, is slightly larger than the value found in the channel flow. We also mention that the values of the ratios between the fourth-order moments of the velocity gradient tensor in THSF at $R_\lambda \approx 145$ are completely consistent with the values obtained in the log-layer of TCF.

Thus, the rotationally invariant fourth moments of the velocity gradient obey simple power laws as a function of y^+ and have ratios very close to the values in HIT or in THSF.

https://doi.org/10.1017/jfm.2016.529 Published online by Cambridge University Press

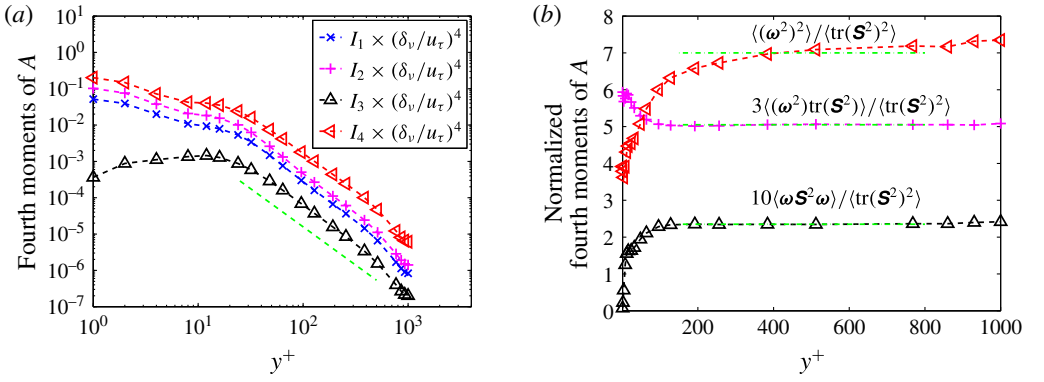


FIGURE 8. (Colour online) The invariant fourth moments of the velocity gradient tensor. (*a*) Variation with the distance from the wall of the four invariants defined by (5.2), normalized by $(u_\tau/\delta_\nu)^4$. Aside from the region close to the wall, where I_3 is much smaller than the other moments, the moments all decay, with a decay law close to y^{+-2}, indicated by the dashed line. (*b*) The ratios I_4/I_1, $3I_2/I_1$ and $10I_3/I_1$. Whereas the ratio I_4/I_1 increases throughout the entire width of the channel, the ratios I_2/I_1 and I_3/I_1 reach approximately constant values, of the order of $I_2/I_1 \approx 1.68$ and $I_3/I_1 \approx 0.235$.

6. Structure of the eigenvalues of the rate of strain matrix

As pointed out by Siggia (1981), the ratios between the moments up to four of the velocity gradient tensor reflect non-trivial properties of the correlation between the eigenvectors of the rate of strain tensor and vorticity; see also Ashurst *et al.* (1987), Tsinober (2009) and Wallace (2009). Since we showed in the previous section that the scalar invariants that completely characterize the moments of the velocity gradient tensor in HIT of order four or less are virtually identical in TCF, it is natural to look in more detail at the strain–vorticity correlation, figure 9(*a*).

We again find very close similarity between HIT and TCF in the PDFs of the cosines between vorticity and the principal axes of the strain. The vorticity is preferentially along the intermediate eigenvector of the rate of strain, i.e. the weak expanding direction, perpendicular to the compressing direction, and does not show any particular alignment with respect to the strong expanding direction; see figure 9(*a*). The agreement between HIT and TCF is even very good for $y^+ = 64$, which is not yet in the log-layer. Finally, the observation that $\boldsymbol{\omega}$ aligns with $\boldsymbol{e}_2$ (see figure 9*a*) on one hand and with $\boldsymbol{e}_{\pi/4}$ (see figure 3*a*) on the other hand points to an alignment between $\boldsymbol{e}_2$ and $\boldsymbol{e}_{\pi/4}$, which is consistent with the results shown in figure 3(*b*).

In turbulent flows, the observation that $\langle \mathrm{tr}(\boldsymbol{S}^3)\rangle < 0$ is related to an asymmetry in the distribution of the eigenvalues of strain. Namely, using the identity deduced from the condition $\lambda_1 + \lambda_2 + \lambda_3 = 0$ that $\lambda_1^3 + \lambda_2^3 + \lambda_3^3 = 3\lambda_1\lambda_2\lambda_3$, a negative value of $\langle \mathrm{tr}(\boldsymbol{S}^3)\rangle$ imposes that, on average, the probability of having two positive eigenvalues of $\boldsymbol{S}$ is higher that the probability of having one positive and two negative eigenvalues; in other words, the intermediate eigenvalue λ_2 is preferentially positive. A common way to quantify this property consists in introducing a dimensionless quantity β,

$$\beta = \frac{\sqrt{6}\lambda_2}{\sqrt{\lambda_1^2 + \lambda_2^2 + \lambda_3^2}}, \tag{6.1}$$

https://doi.org/10.1017/jfm.2016.529 Published online by Cambridge University Press

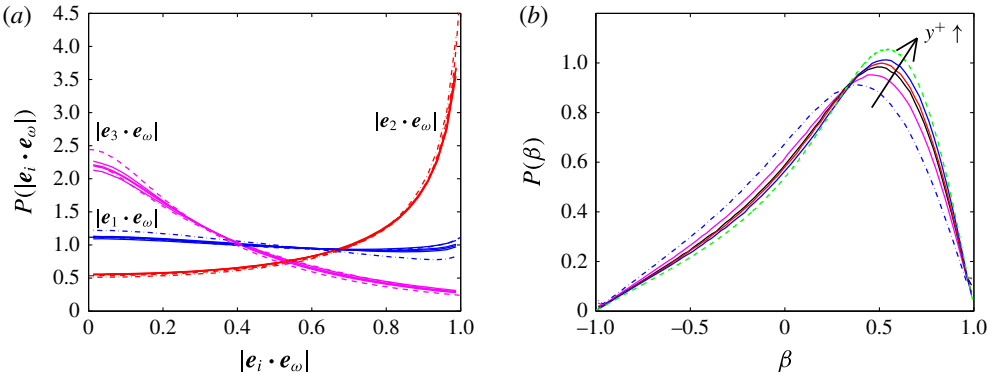


FIGURE 9. (Colour online) Alignment between the eigenvectors of strain and vorticity (*a*) and dimensionless eigenvalue β as defined by (6.1) (*b*). (*a*) The PDF of the scalar product $|\boldsymbol{e}_i \cdot \boldsymbol{e}_\omega|$ is shown at different values of y^+. In the range $128 \leqslant y^+ \leqslant 768$, the PDFs are indistinguishable. Deviations from the universal PDFs are visible in the data for $y^+ = 64$ shown as dashed-dot curves. The dashed lines show the PDFs for HIT. The difference is small, but visible for $|\boldsymbol{e}_3 \cdot \boldsymbol{e}_\omega|$. The PDFs for $|\boldsymbol{e}_2 \cdot \boldsymbol{e}_\omega|$ ($|\boldsymbol{e}_1 \cdot \boldsymbol{e}_\omega|$) almost perfectly superpose with the corresponding PDFs in TCF at $y^+ = 64$ ($y^+ \geqslant 128$). (*b*) The PDF of β at values of $y^+ = 64$ (blue dashed-dot), 128, 256, 512 and 768. The arrow indicates how the PDFs vary as a function of y^+. In the range $y^+ \gtrsim 200$, which corresponds to the log-layer, the curves differ only slightly from the curve for the case of HIT, shown as a green dashed line.

such that $-1 \leqslant \beta \leqslant 1$. The tendency of λ_2 to be preferentially positive leads to an asymmetric PDF of β, as seen many times in simulations of HIT flows.

The PDF of β in the channel flow, shown in figure 9(*b*), at several values of y^+ in the range $64 \leqslant y^+ \leqslant 768$, and for an HIT flow, demonstrate, as expected, that the values of β are preferentially positive. The changes of the PDF of β when y^+ increases, indicated by the arrow in figure 9(*b*), are systematic, but moderate, for $y^+ \gtrsim 100$. The PDF of β at the centre of the channel (not shown) simply extrapolates the trend shown in figure 9(*b*). The PDF in the HIT case deviates only slightly from the PDFs shown in the log-layer of the channel.

7. Discussion and concluding remarks

This article establishes two new facts based on the simulation of TCF available on the Johns Hopkins University Turbulence Database (Li *et al.* 2008; Lee *et al.* 2013; Graham *et al.* 2014):

(i) the skewness of $\partial_y u$ is ~ 1.1 and is constant throughout the log-layer,
(ii) the rotationally invariant vorticity–strain correlations that characterize HIT are virtually unchanged in the log-layer of TCF.

These facts superficially appear contradictory but may point to potent extensions of the classical phenomenological description of wall-bounded shear flow, and certainly invite experimental tests at higher Reynolds numbers and other geometries. We elaborate each in turn.

The restoration of isotropy is an informative characterization of the turbulence state. Phenomenological considerations, following Kolmogorov (Corrsin 1958; Lumley 1967), predict that the effect of anisotropy on the velocity derivatives is of the order

https://doi.org/10.1017/jfm.2016.529 Published online by Cambridge University Press

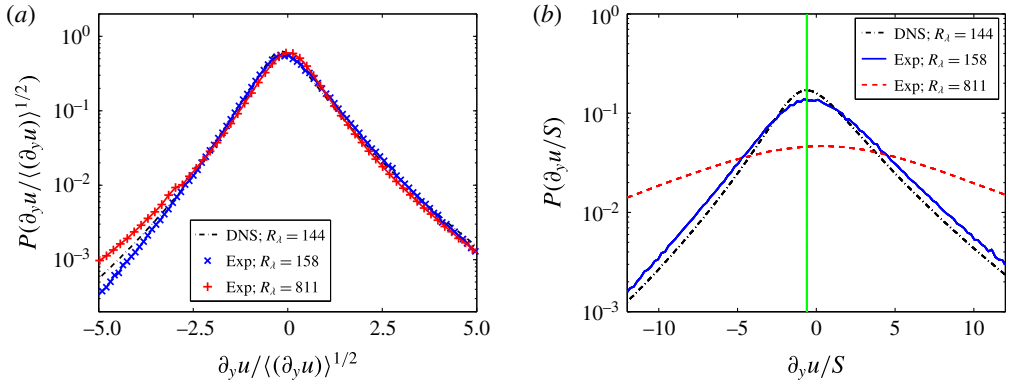


FIGURE 10. (Colour online) Comparison of the PDF of $\partial_y u$ in THSF between moderate-Reynolds-number DNS ($R_\lambda = 144$, dashed–dotted line) and experiment ($R_\lambda = 158$, crosses (*a*) or full line (*b*)) and high-Reynolds-number experiment ($R_\lambda = 811$, plus signs (*a*) or dashed line (*b*)). The experimental data come from Shen & Warhaft (2000) and the numerical data come from simulations of THSF. (*a*) Shows the whole PDF of $\partial_y u$ in units of the root mean square $\langle(\partial_y u)^2\rangle^{1/2}$. (*b*) Shows the PDF of $\partial_y u$ in units of the constant imposed mean shear, $S = U'(y)$. The vertical line corresponds to $\partial_y u/S = -0.6$. The partial expulsion, shown at moderate Reynolds numbers $R_\lambda \lesssim 200$ by the peak of the PDF of $\partial_y u$ at $\approx -0.6S$, disappears when R_λ is much larger. The data shown in this figure are to be compared with the data in TCF, shown at smaller Reynolds numbers in figure 5.

of the ratio of the large-scale gradient to the gradient at the scale of the smallest eddies, which behaves as R_λ^{-1}. This argument correctly predicts how quantities based on the second-order moments of the velocity derivatives return to isotropy at high Reynolds numbers (Pumir & Shraiman 1995; Ishihara, Yoshida & Kaneda 2002; Tsuji 2003; Kaneda, Morishita & Ishihara 2013). Passive scalar advection in a shear flow, however, strongly violates standard theory since the derivative skewness is of order 1 (Sreenivasan 1991; Shraiman & Siggia 2000). Therefore, based on an analogy between scalar transport and momentum transport in a shear, Pumir & Shraiman (1995) simulated THSF and computed $S_{\partial_y u}$. New simulations following Pumir (1996) for THSF at $R_\lambda \sim 144$ very close to TCF show $S_{\partial_y u} \approx 0.8$. Laboratory experiments with active grids provide THSF data up to $R_\lambda \sim 1000$ and suggest $S_{\partial_y u} \propto R_\lambda^{-1/2}$, still a violation of phenomenological theory, but consistent with eventual isotropy.

The PDF of $\partial_y u$ around the origin defines the most probable gradient in the flow. For scalar transport, the PDF peaked at minus the mean external gradient, implying the plateau–step structure seen in single-point data traces. In the simulations of THSF, at Reynolds numbers up to $R_\lambda \approx 145$, the peak of $\partial_y u$ is $\approx -0.6U'$; see figure 10(*b*). When we magnified the data from Shen & Warhaft (2000) around the origin, see figure 10, we found the peak in PDF($\partial_y u$) at $R_\lambda = 158$ to be completely consistent with our numerics, but to move close to 0 at $R_\lambda = 811$. This observation demonstrates a restoration of isotropy of THSF at high enough Reynolds number, consistent with the observed decrease of the skewness of $\partial_y u$ (Shen & Warhaft 2000). For the TCF at $Re_\tau \approx 1000$ studied here, the skewness of $\partial_y u$ is larger than in THSF at a comparable value of R_λ, and constant over the entire log-layer, while the peak in PDF($\partial_y u$) is $\approx -0.7U'(y)$. This is slightly more negative than the value observed for THSF at a comparable R_λ, but note that the PDFs for TCF superimpose very well around the

https://doi.org/10.1017/jfm.2016.529 Published online by Cambridge University Press

origin, even though the mean velocity gradient varies by 6 times over the range of distances from the wall considered; see figure 5.

It is thus very interesting to ask about the behaviour of wall-bounded shear flow at R_τ larger than $\sim$1000 examined here. One might suppose that the flow will approach isotropy like THSF. A more interesting alternative and not implausible outcome in our view is $S_{\partial_y u} \sim 1$ independent of y, and maintained by injection of slowly moving fluid from the wall.

Irrespective of the infinite-Reynolds-number limit, THSF is a useful model for wall-bounded flow, as anticipated by Pumir & Shraiman (1995) (see also Pumir 1996) and further developed by Cardesa *et al.* (2015), Dong *et al.* (2015) and Dong (2016), who observed suggestive analogies between the structures in THSF and those of TCF away from the wall (Theodorsen 1952; Moin & Kim 1985; Head & Bandyopadhyay 1991; Wu & Moin 2009).

Symmetry restricts the number of independent one-point velocity gradient correlations that collectively define the state of HIT. For the second and third moments only one scalar combination of vorticity and strain is allowed by homogeneity. We generalized the argument of Bradshaw & Perot (1993) for $\langle \mathrm{tr}(\boldsymbol{A}^2)\rangle$, and related $\langle \mathrm{tr}(\boldsymbol{A}^3)\rangle$ in TCF to y derivatives of averaged quantities that are small. Thus, the third-order scalar combinations of vorticity and strain in TCF behave as if they were homogeneous isotropic, but of course there will be many non-zero gradient correlations in TCF that violate isotropy or reflection invariance. All isotropic combinations of vorticity and strain vary with distance from the wall very nearly as one would infer from their dimension and the relation for the local dissipation, $\tilde{\epsilon} \sim y^{+-1}$ (Brouwers 2007; Kaneda *et al.* 2013).

The fourth-order scalar invariants of the velocity–strain correlations are not constrained by homogeneity (Siggia 1981). Their ratios in TCF are nearly independent of y and closely approximate the values for HIT or THSF. For HIT there is reasonable evidence that all four invariants scale in the same way with R_λ (Ishihara *et al.* 2007), which also defines the growth in squared dissipation. The observed collapse for $100 < y_+ < 800$ of the distributions of the angles between vorticity and the rate of strain axes onto universal curves that are very close to those of HIT provides a hint that the statistical properties of the scalar invariants of the velocity gradient tensor of order higher than 4 will be similar to those in HIT.

To rephrase the dichotomy with which we began this section, correlations that violate rotation and reflection invariance such as odd powers of $\partial_y u$ seem to be decoupled from those that are invariant under the full rotation group. Both the Kolmogorov energy cascade and the von Kármán boundary layer are theories built around a conserved flux with a scaling regime sandwiched between large and small scales (Tennekes & Lumley 1983). In the related problem of a passive scalar mixed by a turbulent flow, the generation of small scales in the presence of a passive scalar flux leads to a natural decomposition of the moments of the scalar gradient in terms of decomposition of the rotation group $SO(3)$ (Mydlarski *et al.* 1998; Shraiman & Siggia 2000; Falkovich, Gawedzki & Vergassola 2001). Our numerical results may point to a similar property for the velocity gradient tensor in turbulent shear flows.

Acknowledgements

We thank X. Shen and Z. Warhaft for making the original data from Shen & Warhaft (2000) available for us to replot in figure 10, and Z. Warhaft and S. Pope for their comments on an early version of the paper. A.P. acknowledges

https://doi.org/10.1017/jfm.2016.529 Published online by Cambridge University Press

the support from A.N.R. (France) under contract 'TEC 2', and from the Alexander von Humboldt foundation (Germany). E.D.S. was supported by NSF grant PHY 1502151. Computations were performed at the PSMN computing centre at the Ecole Normale Supérieure de Lyon.

REFERENCES

ABE, M., ANTONIA, R. A. & KAWAMURA, H. 2009 Correlation between scall-scale velocity and scalar fluctuations in a turbulent channel flow. *J. Fluid Mech.* **627**, 1–32.

ANTONIA, R. A., ABE, H. & KAWAMURA, H. 2009 Analogy between velocity and scalar fields in turbulent channel flow. *J. Fluid Mech.* **628**, 241–268.

ASHURST, W. M., KERSTEIN, A. R., KERR, R. M. & GIBSON, C. H. 1987 Alignment of vorticity and scalar gradient with strain in simulated Navier–Stokes turbulence. *Phys. Fluids* **30**, 2343–2353.

BETCHOV, R. 1956 An inequality concerning the production of vorticity in isotropic turbulence. *J. Fluid Mech.* **1**, 497–504.

BIFERALE, L. & PROCACCIA, I. 2005 Anisotropy in turbulent flows and in turbulent transport. *Phys. Rep.* **414**, 43–164.

BIFERALE, L. & VERGASSOLA, M. 2001 Isotropy versus anisotropy in small-scale turbulence. *Phys. Fluids* **13**, 2139–2141.

BRADSHAW, P. & PEROT, B. 1993 A note on turbulent energy dissipation in the viscous wall region. *Phys. Fluids* **5**, 3305–3306.

BROUWERS, J. J. H. 2007 Dissipation equals production in the log layer of wall-induced turbulence. *Phys. Fluids* **19**, 101702.

CARDESA, J. I., MISTRY, D., GAN, L. & DAWSON, J. R. 2013 Invariants of the reduced velocity gradient tensor in turbulent flows. *J. Fluid Mech.* **716**, 597–615.

CARDESA, J. I., VELA-MARTIN, A., DONG, S. & JIMENEZ, J. 2015 The temporal evolution of the energy flux across scales in homogeneous turbulence. *Phys. Fluids* **27**, 111702.

CASCIOLA, C. M., GUALTIERI, P., BENZI, R. & PIVA, R. 2003 Scale-by-scale budget and similarity laws for shear turbulence. *J. Fluid Mech.* **476**, 105–114.

CASCIOLA, C. M., GUALTIERI, P., JACOB, B. & PIVA, R. 2007 The residual anisotropy at small scales in high shear turbulence. *Phys. Fluids* **19**, 101704.

CORRSIN, S. L. 1958 Local isotropy in turbulent shear flows. *Tech. Rep.* National Advisory Committee for Aeronautics.

DONG, S. 2016 Coherent structures in statistically-stationary homogeneous shear turbulence. PhD thesis, Universidad Politécnica de Madrid.

DONG, S., LOZANO-DURÁN, A., SEKIMOTO, A. & JIMENEZ, J. 2015 Detached coherent structures in channel revisited: comparison with homogeneous shear turbulence. *Abstract, 15th European Turbulence Conference*. http://www.etc15.nl/proceedings/proceedings/documents/286.pdf.

FALKOVICH, G., GAWEDZKI, K. & VERGASSOLA, M. 2001 Particles and fields in fluid turbulence. *Rev. Mod. Phys.* **73**, 913–975.

FERCHICHI, M. & TAVOULARIS, S. 2000 Reynolds number effects on the fine structure of uniformly sheared turbulence. *Phys. Fluids* **11**, 2942–2953.

FRISCH, U. 1995 *Turbulence*, 1st edn. Cambridge University Press.

GARG, S. & WARHAFT, Z. 1998 On small scale statistics in a simple shear flow. *Phys. Fluids* **10**, 662–673.

GRAHAM, J., LEE, M., MALAYA, N., MOSER, R. D., EYINK, G. & MENEVEAU, C. 2014 The JHU turbulence database: turbulent channel flow data set. http://turbulence.pha.jhu.edu/docs/README-CHANNEL.pdf.

GUALTIERI, P., CASCIOLA, C. M., BENZI, R., AMATI, G. & PIVA, R. 2002 Scaling laws and intermittency in homogeneous shear flow. *Phys. Fluids* **14**, 583–596.

HEAD, M. R. & BANDYOPADHYAY, P. 1991 New aspects of turbulent boundary layer structure. *J. Fluid Mech.* **107**, 297–338.

https://doi.org/10.1017/jfm.2016.529 Published online by Cambridge University Press

HOLZER, M. & SIGGIA, E. D. 1994 Turbulent mixing of a passive scalar. *Phys. Fluids* **6**, 1820–1837.

ISHIHARA, T., KANEDA, Y., YOKOKAWA, M., ITAKURA, K. & UNO, A. 2007 Small-scale statistics in high-resolution numerical simulation of turbulence: Reynolds number dependence of one-point velocity gradient statistics. *J. Fluid Mech.* **592**, 335–366.

ISHIHARA, T., YOSHIDA, K. & KANEDA, Y. 2002 Anisotropic velocity correlation spectrum at small scales in a homogeneous turbulent shear flow. *Phys. Rev. Lett.* **88**, 154501.

KANEDA, Y., MORISHITA, K. & ISHIHARA, T. 2013 Small scale universality and spectral characteristics in turbulent flows. In *International Symposium on Turbulence and Shear Flow Phenomena*. http://www.tsfp-conference.org/proceedings/2013/v1/inv2.pdf.

KIM, J., MOIN, P. & MOSER, R. 1987 Turbulence statistics in fully developed channel flow at low Reynolds numbers. *J. Fluid Mech.* **177**, 133–166.

KOLMOGOROV, A. N. 1941 The local structure of turbulence in incompressible viscous fluid for very large Reynolds numbers. *Dokl. Akad. Nauk SSSR* **30**, 301–305.

KURIEN, S. & SREENIVASAN, K. R. 2000 Anisotropic scaling contribution to high-order structure functions in high-Reynolds-number turbulence. *Phys. Rev.* E **62**, 2206–2212.

LANDAU, L. D. & LIFSHITZ, E. M. 1959 *Fluid Mechanics*, 1st edn. Pergamon.

LEE, M., MALAYA, N. & MOSER, R. 2013 Petascale direct numerical simulation of turbulent chennel flow on up to 768k cores. *Supercomputing (SC13)*. https://www.hpcwire.com/2013/11/15/sc13-research-highlight-petascale-dns-turbulent-channel-flow/.

LI, Y., WAN, M., YANG, Y., BURNS, R., MENEVEAU, C., BURNS, R., CHEN, S., SZALAY, A. & EYINK, G. 2008 A public turbulence database cluster and application to study Lagrangian evolution of velocity increments in turbulence. *J. Turbul.* **9** (31), 133–166.

LUMLEY, J. L. 1967 Similarity and the turbulent energy spectrum. *Phys. Fluids* **10**, 855–858.

MARUSIC, I., MONTY, J. P., HULTMARK, M. & SMITS, A. J. 2013 On the logarithmic region in wall turbulence. *J. Fluid Mech.* **716**, R3,1–11.

MOIN, P. & KIM, J. 1982 Numerical investigation of turbulent channel flows. *J. Fluid Mech.* **118**, 341–377.

MOIN, P. & KIM, J. 1985 The structure of the vorticity field in turbulent channel flow. Part 1. Analysis of instantaneous fields and statistical correlations. *J. Fluid Mech.* **155**, 441–464.

MOSER, R. D., KIM, J. & MANSOUR, N. N. 1999 Direct numerical simulation of turbulent channel flows up to $r_\tau = 590$. *Phys. Fluids* **11**, 943–945.

MYDLARSKI, L., PUMIR, A., SHRAIMAN, B., SIGGIA, E. D. & WARHAFT, Z. 1998 Structures and multipoint correlators for turbulent advection: predictions and experiments. *Phys. Rev. Lett.* **81**, 4373–4376.

POPE, S. B. 2000 *Turbulent Flows*. Cambridge University Press.

PUMIR, A. 1994 A numerical study of the mixing of a passive scalar in three-dimensions in the presence of a mean gradient. *Phys. Fluids* **6**, 2118–2132.

PUMIR, A. 1996 Turbulence in homogeneous shear flows. *Phys. Fluids* **8**, 3112–3127.

PUMIR, A. 1998 Structures of the three-point correlation function of a passive scalar in the presence of a mean gradient. *Phys. Rev.* E **57**, 2914–2929.

PUMIR, A. & SHRAIMAN, B. 1995 Persistent small scale anisotropy in homogeneous shear flows. *Phys Rev. Lett.* **75**, 3114–3117.

SADDOUGHI, S. & VEERAVALLI, S. V. 1994 On small scale statistics in a simple shear flow. *J. Fluid Mech.* **268**, 333–372.

SCHUMACHER, J. & ECKHARDT, B. 2000 On statistically stationary homogeneous shear turbulence. *Eur. Phys. Lett.* **52**, 627–632.

SCHUMACHER, J., SREENIVASAN, K. R. & YEUNG, P. K. 2003 Derivative moments in turbulent shear flows. *Phys. Fluids* **15**, 84–90.

SEKIMOTO, A., DONG, S. & JIMENEZ, J. 2016 Numerical simulation of statistically stationary and homogeneous shear turbulence and its relation to other shear flows. arXiv:1601.01646.

SHEN, X. & WARHAFT, Z. 2000 The anisotropy of the small scale structure in high Reynolds number ($R_\lambda = 1000$) turbulent shear flow. *Phys. Fluids* **12**, 2976–2989.

SHRAIMAN, B. & SIGGIA, E. D. 2000 Scalar turbulence. *Nature* **405**, 639–646.

https://doi.org/10.1017/jfm.2016.529 Published online by Cambridge University Press

SIGGIA, E. D. 1981 Invariants for the one-point vorticity and strain rate correlation functions. *Phys. Fluids* **24**, 1934–1936.

SMITS, A. J. 2010 High-Reynolds number wall turbulence. *Annu. Rev. Fluid Mech.* **43**, 353–375.

SREENIVASAN, K. R. 1991 On local isotropy of passive scalars in turbulent flows. *Proc. R. Soc. Lond.* A **434**, 165–182.

SREENIVASAN, K. R. & ANTONIA, R. A. 1997 The phenomenology of small-scale turbulence. *Annu. Rev. Fluid Mech.* **29**, 435–472.

STAICU, A., VORSELAARS, B. & VAN DE WATER, W. 2003 Turbulence anisotropy and the $SO(3)$ description. *Phys. Rev.* E **68**, 046303.

TENNEKES, H. & LUMLEY, J. L. 1983 *A First Course on Turbulence*, 9th edn. MIT Press.

THEODORSEN, T. 1952 Mechanism of turbulence. In *2nd Midwestern Conference Fluid Mechanics*, pp. 1–19. Columbus Ohio State University.

TONG, C. & WARHAFT, Z. 1994 On passive scalar derivative statisics in grid turbulence. *Phys. Fluids* **6**, 2165–2176.

TSINOBER, A. 2009 *An Informal Conceptual Introduction to Turbulence*, 1st edn. Springer.

TSUJI, Y. 2003 Large-scale anisotropy effect on small-scale statistics over rough wall turbulent boundary layers. *Phys. Fluids* **15**, 3816–3828.

VREMAN, A. W. & KUERTEN, J. G. M. 2014 Statistics of spatial derivatives of velocity and pressure in turbulent channel flow. *Phys. Fluids* **27**, 084103.

WALLACE, J. M. 2009 Twenty years of experimental and direct numerical simulation access to the velocity gradient tensor: what have we learned about turbulence? *Phys. Fluids* **21**, 021301.

WARHAFT, Z. 2000 Passive scalars in turbulent flows. *Annu. Rev. Fluid Mech.* **32**, 203–240.

WARHAFT, Z. & SHEN, X. 2001 Some comments on the small scale structure of turbulence at high Reynolds numbers. *Phys. Fluids* **13**, 1532–1533.

WU, X. & MOIN, P. 2009 Direct numerical simulation of turbulence in a nominally zero-pressure-gradient flat-plate boundary layer. *J. Fluid Mech.* **630**, 4–41.

https://doi.org/10.1017/jfm.2016.529 Published online by Cambridge University Press